ACS OMEGA

http://pubs.acs.org/journal/acsodf

Article

Modulation of α-Chymotrypsin Conjugated to Magnetic Nanoparticles by the Non-Heating Low-Frequency Magnetic Field: Molecular Dynamics, Reaction Kinetics, and Spectroscopy Analysis

Maxim M. Veselov, Igor V. Uporov, Maria V. Efremova, Irina M. Le-Deygen, Andrey N. Prusov, Igor V. Shchetinin, Alexander G. Savchenko, Yuri I. Golovin, Alexander V. Kabanov,* and Natalia L. Klyachko*

Cite This: *ACS Omega* 2022, 7, 20644−20655

Read Online

ACCESS | Metrics & More | Article Recommendations | Supporting Information

ABSTRACT: Enzymes conjugated to magnetic nanoparticles (MNPs) undergo changes in the catalytic activity of the non-heating low-frequency magnetic field (LFMF). We apply in silico simulations by molecular dynamics (MD) and in vitro spectroscopic analysis of the enzyme kinetics and secondary structure to study α-chymotrypsin (CT) conjugated to gold-coated iron oxide MNPs. The latter are functionalized by either carboxylic or amino group moieties to vary the points of enzyme attachment. The MD simulation suggests that application of the stretching force to the CT globule by its amino or carboxylic groups causes shrinkage of the substrate-binding site but little if any changes in the catalytic triad. Consistent with this, in CT conjugated to MNPs by either amino or carboxylic groups, LFMF alters the Michaelis−Menten constant but not the apparent catalytic constant k_{cat} (= $V_{max}/[E]_o$). Irrespective of the point of conjugation to MNPs, the CT secondary structure was affected with nearly complete loss of α-helices and increase in the random structures in LFMF, as shown by attenuated total reflection Fourier transformed infrared spectroscopy. Both the catalytic activity and the protein structure of MNP-CT conjugates restored 3 h after the field exposure. We believe that such remotely actuated systems can find applications in advanced manufacturing, nanomedicine, and other areas.

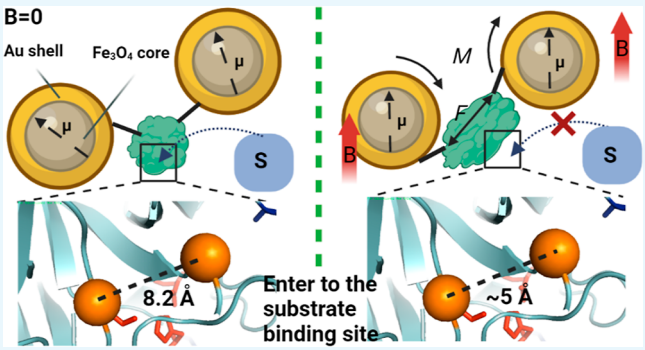

INTRODUCTION

The connection between the structure and function of enzymes is a well-researched area that is critical for mechanistic understanding of biocatalysis. Enzymes are unique protein machines, which accelerate chemical reactions up to 17 orders of magnitude.[1] That tremendous acceleration is explained mainly by the dimensional organization of protein globule and the precise location of the functional groups in the enzyme's active site. The role of the conformational changes in the protein globule during chemical reactions in enzymatic catalysis is still widely discussed.[1−4] The application of the mechanical stimuli to alter the catalytic function has also been sought, but the practical use of such a strategy has been hindered by challenges to precise modulation of the enzyme conformation by the mechanical forces in bulk. Enzyme structure changes responding to external mechanical stimuli were examined by Klibanov and co-authors[5] in the late 1970s for the first time. According to the study, α-chymotrypsin (CT) immobilized onto the elastic support showed reversible loss of activity during support stretching. This approach was called enzymatic mechanochemistry. However, since the mechanical forces were applied to the bulk material, it was unclear to what extent these forces affected the enzyme conformation or whether stretching of the support merely changed the substrate accessibility to the enzyme. Subsequently, the behavior of some enzymes under mechanical stress was studied[6−8] as a result of the development of single molecules manipulation methods such as atomic force microscopy[9,10] and optical[11] or magnetic tweezers.[12] Simultaneous measurements of conformational changes and enzyme activity were also shown[7,8] by combining the magnetic tweezers technique and fluorescence microscopy. This provided estimates of forces that upon application to an enzyme molecule could induce changes in its biocatalytic activity. However, the single molecule approaches did not

Received: February 3, 2022
Accepted: May 25, 2022
Published: June 7, 2022

allow us to affect the enzyme conformation and activity in bulk, which is necessary for various applications.

The solution to this problem was proposed using enzymes conjugated to magnetic nanoparticles (MNPs) and demonstrating that enzymes in such conjugates can undergo changes in catalytic activity in the non-heating low-frequency magnetic field (LFMF).[13] This approach is different from the radio-frequency magnetic hyperthermia that is well documented elsewhere.[14−17] The superparamagnetic MNPs undergo rotational and vibrational motion in the LFMF, which can generate stretching, twisting, and bending forces translated to the macromolecules linked to these nanoparticles, and result in the secondary structure and catalytic activity changes in the conjugated enzyme.[18,19] We term this approach magneto−nanomechanical actuation. By improving the precision of macromolecule attachment to MNPs using modern synthetic chemical or biological conjugation tools, one can possibly achieve simultaneous actuation and control of the biocatalytic function by the remote magnetic field in billions of enzyme molecules in bulk or at the interfaces. To advance our understanding of enzymatic magneto−nanomechanical chemistry, we produced conjugates of CT to gold-coated iron oxide MNPs functionalized by either carboxylic or amino group moieties to vary the points of enzyme attachment. We apply in silico simulations by molecular dynamics (MD) and in vitro spectroscopic analysis of the enzyme kinetics and secondary structure by attenuated total reflection Fourier transformed infrared (ATR-FTIR) spectroscopy to investigate the behavior of these synthetic model systems in non-heating LFMF.

EXPERIMENTAL SECTION

Materials. Iron(II) chloride tetrahydrate ($FeCl_2{\cdot}4H_2O$, 98%), iron(III) chloride ($FeCl_3$), gold(III) chloride trihydrate ($HAuCl_4{\cdot}3H_2O$), sodium citrate trihydrate ($Na_3C_6H_5O_7{\cdot}3H_2O$), citric acid ($C_6H_8O_7$), hydrochloric acid (HCl, 37%), ammonium hydroxide solution ($NH_3{\cdot}H_2O$, 29%), perchloric acid ($HClO_4$, 70%), lipoic acid (LA) ($C_8H_{14}O_2S_2$, 99,9%), cystamine (Cy) dihydrochloride ($C_4H_{12}N_2S_2{\cdot}2HCl$), CT from bovine pancreas, *N*-succinyl-Ala-Ala-Pro-Phe *p*-nitroanilide (NSAAPFpNA), *N*-(3-dimethylaminopropyl)-*N*′-ethylcarbodiimide hydrochloride (EDC), sulfo-*N*-hydroxysuccinimide (S-NHS), tris(hydroxymethyl)aminomethane (TRIS), and 4-nitrophenyl trimethylacetate were all purchased from Sigma-Aldrich. The Micro BCA Protein assay kit was purchased from Thermo Fisher Scientific. 1,4-Dioxane (98%) and acetonitrile (98%) were obtained from Kriochrom (Russia). For all experiments, deionized (DI) water (18,2 MΩ·cm Werner Easypure II system) was used.

MNP Synthesis and Functionalization. MNPs were synthesized, as previously described[18] (see the Supporting Information) by co-precipitation of Fe(II) and Fe(III) salts and then coated with the gold shell by citrate reduction of $HAuCl_4$. After that, the reaction mixture was centrifugated to separate non-coated nanoparticles. For the surface functionalization, 12 mL of purified gold-coated MNPs dispersed in citrate buffer was mixed with 12 mL of 1 mg/mL LA or 1 mg/mL Cy, stirred overnight at room temperature (r.t.), and then dialyzed three times against DI H_2O for 6 h.

Preparation of the MNP-CT Conjugates. CT was conjugated to functionalized MNPs using EDC/S-NHS chemistry using a one-step procedure. (A) MNP-LA-CT: 4 mL of MNP-LA dispersion in DI H_2O were mixed with 2.66 mL of 20 mM citrate buffer (pH 4.5), 3.34 mg of CT, 0.2 mg of EDC, and 0.21 mg of S-NHS. The reaction mixture was stirred for 1.5 h at r.t., and the MNP-LA-CT was separated by centrifugation (3× times, 4800*g*) and dissolved in the citrate buffer. (B) MNP-Cy-CT. Two and four-tenths milliliter of MNP-Cy were mixed with 0.8 mL of 20 mM citrate buffer (pH4.5), 200 μg of CT, 0.4 mg of EDC, and 0.42 mg of S-NHS. The next steps were like mentioned in (a).

Protein Assay. The total amount of immobilized CT was determined using the Micro BCA Protein assay kit (Thermo Fisher Scientific). 150 μL of assay reagents was added to 150 μL of MNP-LA-CT or MNP-Cy-CT dispersion. The mixture was intensely stirred in the shaker for 30 s and then incubated at 37 °C for 2 h. After that, the solution absorbance was measured at 562 nm, and conjugated enzyme quantity was determined from the linear calibration graph for native CT (2−40 μg/mL range).

Active Site Titration. The concentration of the enzyme's active sites ($[E_0]$) was determined using ultraviolet−visible (UV−vis) spectroscopy by measuring the burst of 4-nitrophenol in a reaction of hydrolysis of 4-nitrophenol trimethylacetate by native CT.[20] The time dependence of the product formation was recorded at 400 nm using a molar extinction coefficient ε = 18,500 M^{-1} cm^{-1} and used for determining $[E_0]$ by approximation of the steady-state regime to the zero-time point (Figure S1).

Enzymatic Activity. Enzymatic activity of immobilized CT was determined by UV−vis spectroscopy by measuring the initial rates of hydrolysis of a specific substrate, NSAAPFpNA. The time dependence of the product formation was recorded at 405 nm. The test tubes containing immobilized CT suspensions in 20 mM Tris-HCl buffer (pH 8.2) were placed into an LFMF generator with temperature control (TOR 01/12, Nanodiagnostics LLC, Russia, for more detail see the Supporting Information). The samples were exposed to 50 Hz 140 mT LFMF applied in three 1 min pulses separated by 30 s no field pauses (total of 3 min of field exposure). The temperature during the field exposure remains constant within ∼0.1 K precision of the temperature measurement. After that, the sample aliquots were rapidly placed into microplates and supplemented with 2 μL of 0.1−10 mM substrate solutions in a 1:1 (v/v) dioxane−acetonitrile mixture. The kinetic curves were recorded for 3 min using the SpectraMax M5 (Molecular Devices, USA) UV−vis spectrometer. Changes in the product concentration were determined using ε = 9500 M^{-1} cm^{-1},[21] and the dependence of the initial rate on the substrate concentration was plotted in Lineweaver−Burk plots.

ATR-FTIR Spectroscopy. FTIR spectra were recorded using a Tensor 27 (Bruker, Germany) spectrometer equipped with a liquid cooled mercury−cadmium−telluride detector. Measurements were conducted in a thermostatic cell BioATR II with a ZnSe attenuated total reflection element (Bruker, Germany) at 22 °C. The spectrometer was purged with a constant flow of dry air. The 20× concentrated protein samples (30 μL) were placed on the crystal element, and FTIR spectra from 4000 to 950 cm^{-1} with 1 cm^{-1} spectral resolution were recorded three times. For each spectrum, 70 scans were accumulated and averaged. The baseline was recorded in the same way. Spectral data were processed using Bruker software Opus 7.0. The Amide I region was deconvoluted, and components were defined by the second derivative. The Lorentz form of the fitted curves and Levenberg−Marquardt algorithm of fitting analysis were used, and the number of

https://doi.org/10.1021/acsomega.2c00704
ACS Omega 2022, 7, 20644−20655

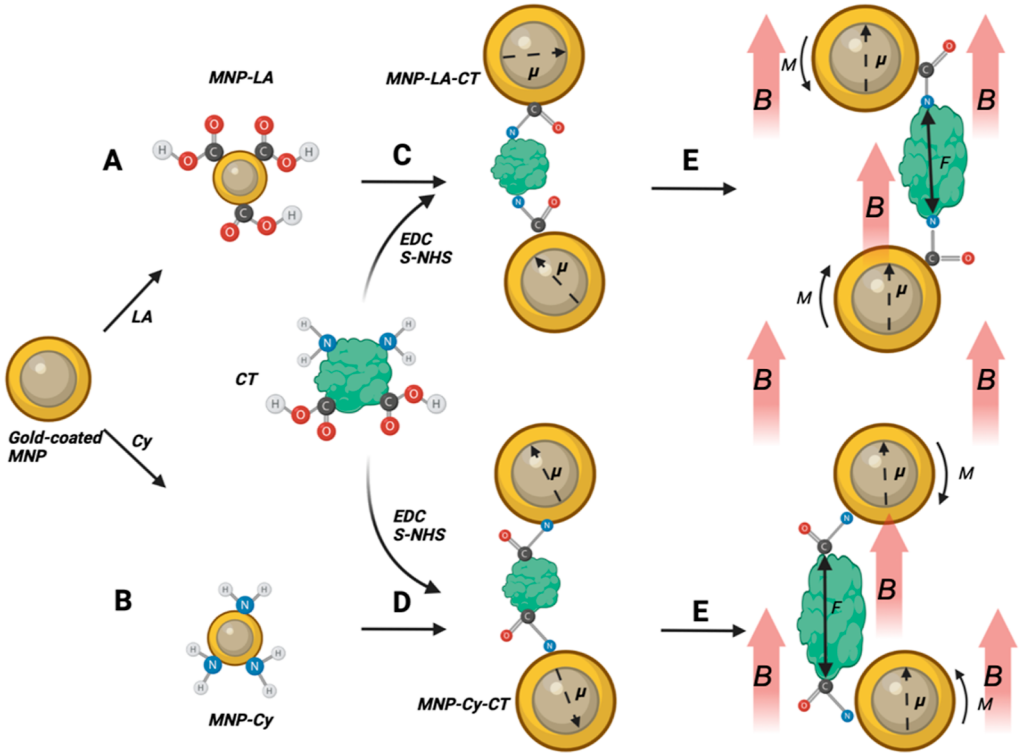

Figure 1. Schematic presentation of the magneto−nanomechanical approach. (A,B) Gold-coated MNPs are modified with (A) LA or (B) Cy to introduce carboxylic or amino groups, resulting in MNP-LA and MNP-Cy, respectively. (C) Surface carboxylic groups of MNP-LA are conjugated to ε-amino groups of lysine in a CT molecule to produce MNP-LA-CT conjugates. (D) Surface amino groups of MNP-Cy are conjugated to carboxylic groups of a CT molecule to produce MNP-Cy-CT. In both cases, the conjugation reactions are carried out in situ using EDC/S-NHS chemistry. (E) Exposure of the MNP-CT conjugates to LFMF results in the generation of forces F applied to different sites in CT. Red arrows show the direction of the LFMF vector B, μ—magnetic moment of MNPs, and M—torque of MNPs. The scheme is simplified and does not present compressing and bending deformation forces. The bending forces could be substantial since the torque would be concentrated not at the large MNP (~25 nm) but at much smaller protein globule (~2 nm). The figure is a schematic representation for clarity and does not correctly reflect the relative sizes of the MNP and protein, heterogeneity of the MNP population, and possible formation of the mixture of structures such as MNP linked to multiple enzyme molecules or enzymes cross-linked to each other. This figure was created with BioRender.com.

components was minimized so that the error was less than 0.05.

Molecular Modeling. The molecular modeling protocol was like that described in detail in our previous work[18] except for the choices of residues to which the forces were applied. Briefly, the radial, directed out of protein center, 80 pN forces were applied here to (1) N_ε atoms of Lys-79, 90, 107, 175, and 202 or (2) to C_β atoms of Asp-21, 49 and C_δ atoms of Glu-64, 129. The CHARMM27 force field was used for simulations and 300 K and other standard simulation parameters.[22] The VMD/NAMD program package was used for MD simulations and analysis of obtained trajectories. System conformations were saved every 5 ps during the MD simulations of 20 ns total length.

Sample Characterization. A transmission electronic microscope JEM 1400, 120 kV (JEOL, Japan) was used to examine the size and morphology of MNPs. Samples for transmission electron microscopy (TEM) were dropped and dried onto a copper 200 mesh grid. Average MNPs' size was determined by analyzing at least 50 particles using ImageJ software (National Institutes of Health, USA). Determination of hydrodynamic size by nanoparticle tracking analysis (NTA) was carried out using a NanoSight NS500 instrument (Malvern, UK) equipped with an 80 mW 532 nm laser. The size distribution of MNPs was determined using NanoSight 2.3 software (Malvern, UK). The zeta-potential of MNPs was measured by dynamic light scattering (DLS) using a ZetaSizer Nano ZS (Malvern, UK), averaging 20 runs measurement using the Smoluchowski model. Samples for DLS were solved in 10 mM KCl solution; the measurements were taken using a transparent zeta-potential cell (DTS1060C). Mössbauer spectra of ^{57}Fe nuclei at room temperature were recorded with a MS-1104Em spectrometer (Southern Federal University, Research Institute of Physics, Russia) in transmission geometry with a ^{57}Co(Rh) radiation source. Spectra analysis was performed by Univem MS program, and the relative intensities (area) of elementary spectra were determined.

RESULTS

The magneto−nanomechanical approach implemented in this study involves the conjugation of different amino acid residues of CT to MNPs followed by application of mechanical forces to the protein globule due to the mechanical motion of the MNPs in the LFMF. Figure 1 illustrates two different synthetic routes, in which the gold-coated MNPs are attached to either the amino or carboxylic groups of the CT. The external LFMF will generate mechanical forces applied to either carboxylic or amino groups of the CT molecule. Here, we (1) carried out the computer modeling to assess the effects of the forces on the CT structure, (2) prepared the conjugates using two different synthetic strategies, and (3) assessed the effects of the

https://doi.org/10.1021/acsomega.2c00704
ACS Omega 2022, 7, 20644−20655

LFMF on the catalytic properties and secondary structure of the enzyme using UV−vis and ATR-FTIR spectroscopies.

Computer Modeling of CT Behavior under Stretching Forces. We posit that the carboxylic or amino groups exposed at the protein surface are available for the conjugation reactions (Figure 1C,D). Analysis of the surface distribution of the charged groups in the CT molecule obtained from the Protein Data Bank (code 1ACB) suggests that all the Lys residues (14) are exposed to the solvent area of at least 50 Å^2. However, only 12 of these residues are available for conjugation as the amino groups of Lys-84 and Lys-107 form hydrogen bonds. These 12 residues are clustered in five sites at the CT surface. Therefore, our modeling applied stretching forces to these five sites of the protein molecule, specifically at Lys-79, 90, 107, 175, and 202. Concerning the stretching of CT via its carboxylic groups, only eight carboxylic groups are exposed to the solvent area of at least 50 Å^2 (Glu-20, 21, 49, Asp-64, 128, 129, 153, and 178). The δ-carboxylic group of Glu-20 forms a hydrogen bond with the OH-group of Ser-11 and, therefore, cannot be conjugated. Two of the remaining seven surface carboxylic groups, Asp-128 and Asp-129, are near each other. Thus, the modeling applied stretching forces to only four sites of the protein molecule at Glu-21, 49, Asp-64, and 129.

The CT behavior under the application of radially directed forces was modeled by the MD using three different protocols: (1) "non-stretched", (2) "NH_2-stretched", and (3) "COOH-stretched." The first, non-stretched protocol implied that the enzyme molecule is placed into a spherical water drop, and no forces are applied. The NH_2-stretched protocol considered an enzyme molecule in a water shell under 80 pN forces radially directed (from the molecule center) and applied to N_ε-atoms of Lys surface residues. The stretching force value in MD simulation is matched with theoretically calculated force values generated by MNPs in LFMF.[19] Finally, the COOH-stretched protocol assumed that these forces are applied to the carbon atoms of carboxylic side groups of Glu and Asp. In both cases, we ensured that the applied forces did not shift the CT molecule from its original position. This was accomplished by proper selection of amino acid residues to ensure that the net force and force moment approached zero. This abolished the need of getting the protein back to the starting position and orientation and simplified the calculation during the modeling. The MD's simulation trajectory length was 20 ns with 5 ps steps.

In both cases, the applied external forces did not lead to a significant distortion of the CT globular structure and the unfolding of the polypeptide chain. The visual analysis of the trajectories indicated that the protein globule is rather stiff (Movies S1−S3). We observed "straightening" of the side chains of the residues to which external forces were applied and local conformational changes in the polypeptide chain in the vicinity of these residues.

The overall CT molecule dynamics in MD simulation is characterized by the time dependency of the protein structure deviation from its initial X-ray structure (Figure 2). As a measure of this deviation, we used the root-mean-square deviation (rmsd) of backbone heavy (C, N, O) atoms. The rmsd (Å) was calculated according to

$$\text{rmsd} = \frac{\sum_{i-1}^{N} d_i^2}{N}$$

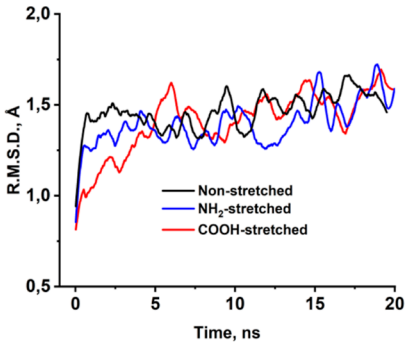

Figure 2. Time dependency of rmsd for heavy atoms (excluding hydrogen) of the CT polypeptide chain from the initial X-ray structure. The external forces of 80 pN were applied radially to (1) N_ε atoms of Lys-79, 90, 107, 175, and 202 (NH_2-stretched) or (2) C_β atoms of Glu-21, 49 and C_δ atoms of Asp-64, 129 (COOH-stretched) or not applied (non-stretched). The initial X-ray structure was obtained from the Protein Data Bank (code 1ACB). The data are smoothed by the second-order Savitzky−Golay method with 50 points window.

where d_i is the distance between heavy atom i of the backbone of the CT molecule and its position in the initial X-ray structure, and N is the total number of equivalent atoms. Consistent with our visual observation, there were practically no deviations in the rmsd values for both stretched protocols from those values in the absence of stretching. However, in every protocol (stretched or non-stretched), we observed slight deviations of these values from the initial X-ray structure, suggesting a slight structural drift of the protein structure in the course of MD simulation. This deviation develops rapidly within the first few picoseconds from the onset of the simulation and then nearly levels off at ∼1.5 to 1.6 Å.

For the in-depth analysis of the dynamic changes in the CT molecule that could potentially affect the enzyme functional activity, we focused on the structural changes in the catalytic triad and the substrate-binding site. The catalytic triad presented by Ser-195, His-57, and Asp-102 residues in the CT molecule is the site where the conversion of substrate into product occurs. The correct spatial arrangement of these residues in the vicinity of each other is essential for effective catalytic function. The deviation from this arrangement because of the changes in protein conformation under applied forces could result in changes in the enzyme's catalytic activity. Here, we used the distances between pairs (1) His-57:$N_{\delta1}$ and Asp-102:$O_{\delta2}$ and (2) His-57:$N_{\varepsilon2}$ and Ser-195:O_γ as a measure of such deviations in the catalytic triad. The MD modeling was run for 20 ns with 5 ps steps yielding 4000 measurements in each modeling run. This allowed us to construct the distribution function of the distances (DF) for each of the (1) non-stretched, (2) NH_2-stretched, and (3) COOH-stretched protocols, as presented in Figure 3. In the absence of the applied force, the DF for His-57:$N_{\delta1}$ and Asp-102:$O_{\delta2}$ (Figure 3A) reveals one relatively narrow peak, suggesting slight (∼0.2−0.3 Å) fluctuations of the distance between these residues near its X-ray value (∼2.9 Å). A widening of the distribution is observed upon application of forces, especially for the COOH-stretching, where a second broad peak is revealed at ∼3.45 Å. There is a possibility for rotation of a carboxylic group of Asp-102, which possibly leads to the DF widening and appearance of the second peak, as shown in Figure 3A. The first and the second peak, in this case,

https://doi.org/10.1021/acsomega.2c00704
ACS Omega 2022, 7, 20644−20655

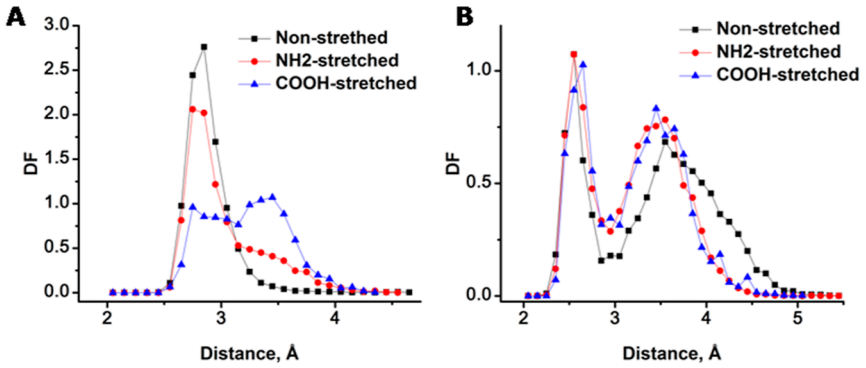

Figure 3. DF between atoms of the catalytic triad (Ser-195, His-57, and Asp-102) in the CT molecule: (A) His-57:$N_{\delta 1}$ and Asp-102:$O_{\delta 2}$ and (B) His-57:$N_{\varepsilon 2}$ and Ser-195:O_{γ}. The external forces of 80 pN were applied, as described in Figure 2, and the analyzed trajectory length was 20 ns. The data for the NH_2-stretched protocol, as shown in the figure, was previously published by us in ref 18.

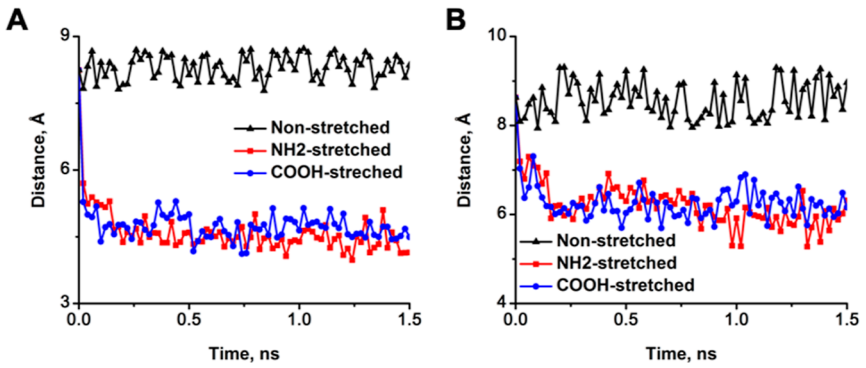

Figure 4. Evolution of the distance between C_{α} atoms in the amino acid residues forming the entrance into the substrate-binding site of the CT molecule: (A) Cys-191:C_{α}-Ser-217:C_{α} and (B) Cys-191:C_{α}-Ser-218:Cα. The external forces of 80 pN were applied, as described in Figure 2. The data for the NH_2-stretched protocol, as shown in the figure, was previously published by us in ref 18. Here, we present only the first 1.5 ns of the MD; full curves are presented in Figure S3.

correspond to two conformations, in which the hydrogen bonds between His-57:$N_{\delta 1}$ and Asp-102:$O_{\delta 1}$ or Asp-102:$O_{\delta 2}$ are formed. From the functional activity point of view, the tight contacts between the His-57:$N_{\delta 1}$ atom and any oxygen of the carboxylic group in these confirmations are equivalent. We would like to point out here a limitation of our modeling approach. It returns the DF corresponding to the evolution of the CT conformation starting from the initial single-crystal structure over a specific observation time. In real life, of course, both conformations are realized, and they are indistinguishable. Therefore, the interpretation of the observed phenomenon is that under our approach and assumptions, the transitions between two different conformations become faster and realize within 20 ns timeframe. Notably, we also observed a shift of the first peak to ∼2.75 Å for both NH_2- and COOH-stretching.

The DF for the His-57:$N_{\varepsilon 2}$ and Ser-195:O_{γ} pair in the absence of force reveals two characteristic peaks at ∼2.85 and ∼3.85 Å (Figure 3B). It was shown previously that the first one corresponds to an active catalytic triad conformation and is observed in the X-ray structure (∼2.9 Å), while the second one is referred to as inactive.[23] Upon COOH-stretching, the DF appears to shift the position of the second peak to ∼3.75 Å, while the first peak is affected much less. Therefore, we would not expect considerable change in the catalytic activity of CT as a result of observed alterations in either His-57:$N_{\delta 1}$ and Asp-102:$O_{\delta 2}$ or His-57:$N_{\varepsilon 2}$ and Ser-195:O_{γ} arrangements upon application of the stretching forces.

To assess the effect of the applied forces on the substrate-binding site, we analyzed the variation of the distances between (1) Cys-191:C_{α} and Ser-217:C_{α} atoms and (2) Cys-191:C_{α} and Ser-218:C_{α} atoms located in the entry to the hydrophobic pocket in the substrate-binding site (Figure S2). The corresponding trajectories are shown in Figure 4. Under the external forces, the distances between corresponding atoms rapidly (0.2−0.3 ns) decrease from 8.2 Å to ∼5 + 1 Å for Cys-191:C_{α} and Ser-217:C_{α} pair and from ∼8.6 Å to ∼6 + 1 Å for Cys-191:C_{α} and Ser-218:C_{α} pair. Similar patterns are observed for both NH_2- and COOH-stretching, while no changes are seen in the absence of the applied force. A visual analysis of the trajectories made it possible to characterize these changes as a "collapse" of the polypeptide chain segments forming the entrance into this pocket. That is supposed to lead to the closure of entrance into the substrate-binding pocket with side chains of corresponding parts of the polypeptide chain and could affect the substrate binding. We have then proceeded to evaluate these predictions experimentally.

Preparation and Characterization of MNP-CT Conjugates. For the experimental validation of theoretical modeling results, we used the core−shell MNPs with the iron oxide core surrounded by the gold shell. These nanoparticles were prepared in a two-step procedure involving synthesis of the magnetic iron oxide nanoparticles by the co-precipitation technique followed by their gold coating, as described before.[13,24] The diameter of the magnetic core and entire gold-coated MNPs were 9 ± 2 nm and 25 ± 3 nm,

https://doi.org/10.1021/acsomega.2c00704
ACS Omega 2022, 7, 20644−20655

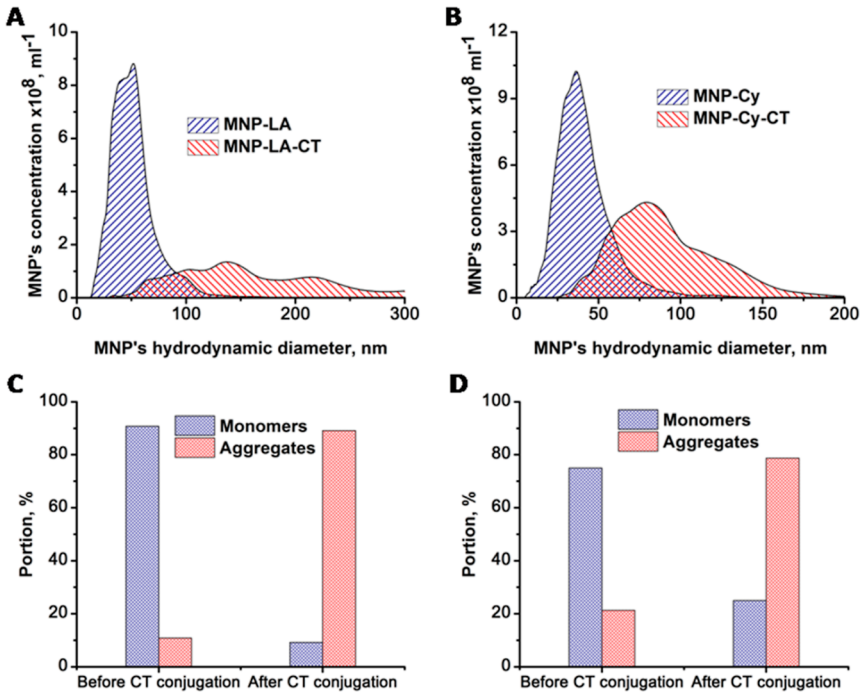

Figure 5. Characterization of functionalized MNPs and MNP-CT conjugates. (A,B) Distribution of the hydrodynamic sizes of the functionalized MNPs and MNP-CT conjugates obtained by the NTA method. (C,D) Change in the fraction of monomeric and aggregated nanoparticles before and after conjugation of (C) MNP-LA and (D) MNP-Cy with CT. The fractions were estimated based on the analysis of TEM micrographs. Each sample group contained 54−378 species.

respectively, based on the TEM of the uncoated and final nanoparticles (Figure S4). The magnetite/maghemite ratio for the synthesized iron oxide nanoparticles was 2/1 based on the analysis of Mossbauer spectra (see Supporting Information, Figure S5 and Table S1). Based on the diameter of the magnetic core, we expect that such nanoparticles subjected to the external LFMF could undergo relaxation by both Neel's and Brown's mechanisms, with the latter mechanism becoming predominant for the particle sizes above a certain critical value, R_c.[25,26] The Brownian relaxation mechanism is essential for the magneto−nanomechanical stimulation of macromolecules.[19] Despite the previous estimate for the critical radius R_c of ∼7 nm,[19,27] our recalculation using magnetic anisotropic constant, K_{eff}, present in the literature,[28,29] resulted in a smaller value of ∼4.1 nm for magnetite and ∼5.9 nm for maghemite (see Supporting Information, Figure S6). These R_c values represent the higher estimates for the critical radius since we used K_{eff} for 10 nm MNPs. Our MNP cores are ca. 9 ± 2 nm in diameter, which could lead to some increase in the K_{eff} and smaller values for the critical radius. Given the size, polydispersity of our MNPs at least a part of them appears to be within the proper size range for the Brownian relaxation mechanism.

The gold shell surrounding the MNPs provides the opportunity for an easy modification of MNPs' surface via thiol or disulfide ligands,[30] increases the stability of MNPs, and protects the MNP magnetic core against oxidation. In this work, we functionalized gold-coated MNPs with two disulfide ligands, (1) LA (MNP-LA) and (2) Cy (MNP-Cy), containing carboxylic and amine groups, respectively (Figure 1A,B). The functionalized MNPs were negatively charged (average zeta-potentials −30.1 ± 6.9 mV MNP-LA and −14.5 ± 1.0 mV MNP-Cy) and stable in aqueous dispersion, as determined by NTA (Figure S7). Next, CT was conjugated to functionalized MNPs using EDC/S-NHS chemistry. In the case of MNP-LA, the surface carboxylic groups formed the amide bonds with accessible ε-amine groups of Lys in CT (Figure 1C). In the case of MNP-Cy, the surface amine groups formed amide bonds with accessible carboxylic groups of Asp and Glu in CT (Figure 1D). The conjugation was a one-step procedure with in situ activation of carboxylic groups by EDC/S-NHS that reacted with the free amino groups. Thus, we synthesized two types of MNP-CT conjugates where either (1) amine (MNP-LA-CT) or (2) carboxylic groups (MNP-Cy-CT) of CT molecules were attached to the MNPs via amide bonds.

Following the conjugation, we observed an increase in the hydrodynamic size of the nanoparticles by 2.5−3.2-fold based on NTA measurements of functionalized MNPs and MNP-CT conjugates (Figure 5A,B, Table 1). From that, we estimate that the portion of enzyme molecules was coupled simultaneously with at least two different MNPs. This estimate was further reinforced by analysis of TEM micrographs (Figures 5C,D and S8), where the assembly of MNPs after conjugation reaction was observed. It should be noted that the conjugation scheme in Figure 1C,D, is simplified and does not present the relative sizes of the MNP and protein, heterogeneity of the MNP population, as well as possible formation of the mixture of structures, such as MNP linked to multiple enzyme molecules,

Table 1. Mean Hydrodynamic Diameters of Functionalized MNPs and MNP-CT Conjugates, Obtained by NTA Measurements[a]

MNP-LA	MNP-LA-CT	MNP-Cy	MNP-Cy-CT
53 ± 0.6 nm	171 ± 3.9 nm	44 ± 0.7 nm	113 ± 1.6 nm

[a]The values are presented as mean ± standard error of mean = SD/$\sqrt{N}$, where N is the value of completed nanoparticles tracks during measurements.

https://doi.org/10.1021/acsomega.2c00704
ACS Omega 2022, 7, 20644−20655

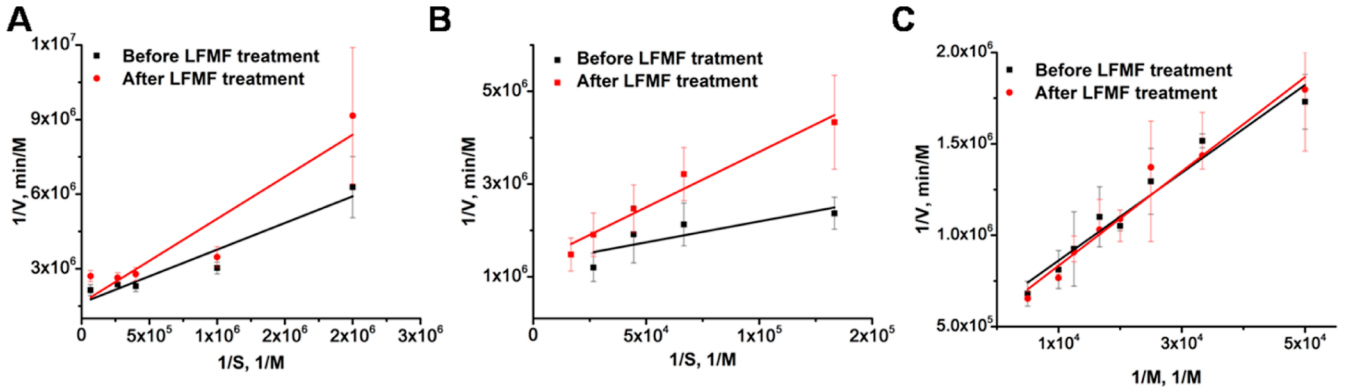

Figure 6. Lineweaver–Burk plots for initial reaction rates (V) of NSAAPFpNA hydrolysis by (A) MNP-LA-CT, (B) MNP-Cy-CT conjugates, and (C) native CT before and after application of LFMF (f = 50 Hz and B = 140 mT). 20 mM Tris-HCl buffer (pH 8.2), 0.5% acetonitrile, 0.5% 1,4-dioxane, and 25 °C. The magnetic field was applied in three 1 min pulses separated by 30 s "no field" intervals.

and/or enzymes cross-linked to each other. It was suggested that the coupling of enzyme molecule simultaneously with at least two MNPs is favorable for magneto–nanomechanical stimulation of enzyme molecules because such arrangement should result in greater deformation forces applied to these molecules.[23]

Effect of the LFMF Exposure on the Enzymatic Activity of MNP-Immobilized CT. We evaluated the effect of applied LFMF on the enzymatic hydrolysis of a specific CT substrate, NSAAPFpNA, in the presence of MNP-CT conjugates. The magnetic field (f = 50 Hz, B = 140 mT) was applied in three 1 min pulses separated by 30 s "no field" intervals. We used the pulsed field regime because it produces a greater effect on the conformation and activity of the enzymes immobilized on MNPs.[13,25] Immediately after the field exposure, the colorimetric reaction was initiated by adding the substrate, and the initial reaction rates of p-nitroaniline formation were recorded by UV–vis spectrometry. It is worth noting that the substrate hydrolysis in the absence of the enzyme was negligible in comparison with the enzymatic hydrolysis (Figure S9). As a result of the field exposure, the initial reaction rate of substrate hydrolysis by MNP-CT conjugates decreased. This was manifested by a decrease in the slopes of the kinetic curves (Figure S10). The kinetic parameters of the reactions (Michaelis–Menten constant K_M and catalytic constant k_{cat}) were determined using Lineweaver–Burk plots (Figure 6). The concentration of the active enzyme $[E]_o$ in the unconjugated CT was determined by the active site titration using 4-nitrophenyl trimethylacetate as a substrate[20] (Figure S1). This value was used to estimate the k_{cat} (= $V_{max}/[E]_o$) in the free enzyme. For the MNP-CT conjugates, we did not have sufficient enzyme concentration for the active centers' titration. Therefore, we used the same $[E]_o$ value for the native enzyme to estimate the $V_{max}/[E]_o$ for the conjugate. This approach did not account for the change in the CT active centers, and therefore, $V_{max}/[E]_o$ for the conjugate is an apparent catalytic constant.

Table 2 presents the kinetic parameters for the native CT and MNP-CT conjugates. In the case of the native enzyme, the K_M was in good agreement with the values published in the literature (43 mM[31]). However, the k_{cat} measured in our experiment was nearly 40% higher compared to the literature (2100 min^{-1}[31]) (which we still consider a reasonably good agreement given an error of the active center titration). Conjugation of CT to MNPs resulted in ∼11 to ∼12-fold decrease in the $V_{max}/[E]_o$, which is likely due to a decrease in the kinetically active centers remaining after the reaction. Surprisingly, the apparent K_M was also decreased by as much as ∼30 (MNP-LA-CT) and ∼6 (MNP-Cy-CT) times. This suggests an increase in the apparent binding affinity of a substrate to the nanoparticle-immobilized enzyme. Notably, similar phenomena have been previously described for various enzymes immobilized on gold nanoparticles. For example, after lipase adsorption on gold nanoparticles, a 2.6-fold decrease in K_M (and no change in V_{max}) was reported.[32] Another study reported both an increase (up to 4.4 times) and a decrease (up to 2.8 times) in K_M values for CT adsorbed on glutamic acid-functionalized gold nanoparticles.[33] This magnitude and sign of this effect were dependent on the substrates' charge interactions with the nanoparticles. In this study, $V_{max}/[E]_o$ was also either decreased (up to 24 times) or increased (up to 3.7 times), depending on the substrates' charge. Finally, a 1.5-fold decrease in K_M and a 5.7-fold increase in V_{max} were seen after covalent attachment of glucose oxidase to gold nanoparticles coated by 11-mercaptoundecanoic acid.[34] In our case, the functionalized MNP-LA and MNP-Cy used for the conjugation were negatively charged (MNP-LA zeta-potential was considerably more negative than that of MNP-Cy). The substrate, NSAAPFpNA, was positively charged (proline NH_2-group pK_a = 10.64[35]). Since the conformation of CT after immobilization practically did not change (as described below), the increases in apparent Michaelis–Menten constant of the conjugates could be explained by the concentration of the substrate due to the charge interactions with functionalized MNPs. This seems to be consistent with considerably lower K_M of MNP-LA-CT, which is derived from more negatively charged functionalized MNPs than MNP-Cy-CT.

Table 2. Effect of the LFMF on Kinetic Parameters of Native or Conjugated CT (Based on Figure 6)

	K_M, μM		$V_{max}/[E]_o$, min^{-1}[a]	
sample	before LFMF	after LFMF	before LFMF	after LFMF
native CT	39 ± 5	45 ± 5	2901 ± 246	3132 ± 278
MNP-LA-CT	1.3 ± 1.0	2.1 ± 1.4	234 ± 51	234 ± 11
MNP-Cy-CT	7 ± 4	18 ± 3	263 ± 67	263 ± 39

[a] $V_{max}/[E]_o$ based on the titration of the active centers in the native CT; equals k_{cat} for the native CT.

https://doi.org/10.1021/acsomega.2c00704
ACS Omega 2022, 7, 20644–20655

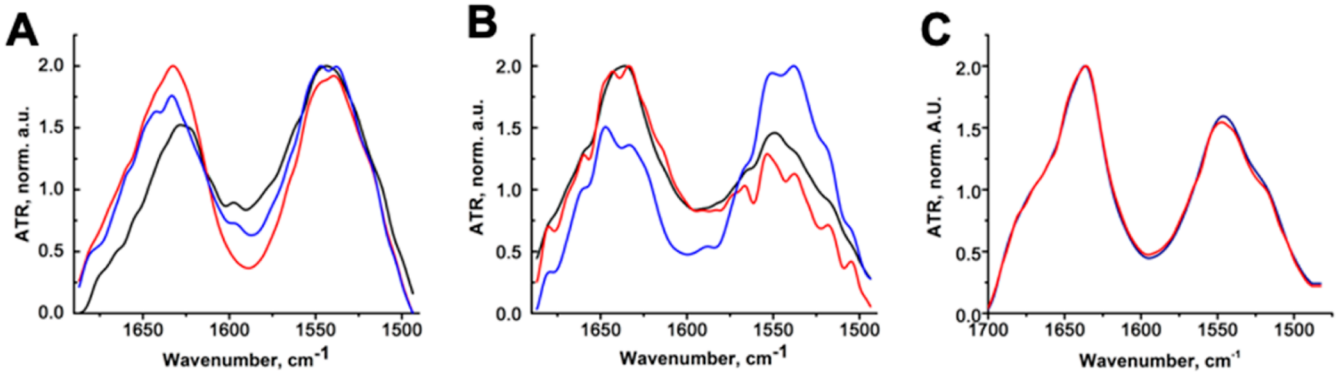

Figure 7. Amide bond absorption region of (A) MNP-LA-CT, (B) MNP-Cy-CT conjugates, and (C) native CT (0.5 mg/mL) before (black line), immediately after (red line), and 3 h after (blue line) LFMF exposure. Spectra are normalized. Conjugated CT samples were ×20 concentrated after synthesis.

The exposure of both conjugates to LFMF had no effect on k_{cat}. However, we observed, respectively, ∼1.6- and ∼2.5-fold increase in K_M for MNP-LA-CT and MNP-Cy-CT. We want to point out that the K_M for MNP-LA-CT in the presence of the field is dependent on the low substrate concentration point and has a greater error compared to K_M for MNP-Cy-CT based on the Lineweaver−Burk plots, as shown in Figure 6. However, the differences in K_M with and without field for MNP-Cy-CT are clear for the entire range of the substrate concentration. Interestingly, 3 h after the magnetic field exposure, the enzymatic activity in the MNP-CT conjugates partially restored (Figure S11). There was no effect of LFMF on the free CT. The changes in the kinetic parameters of MNP-CT conjugates are consistent with the MD prediction that the deformation forces applied to CT affects the substrate-binding site but not the catalytic triad.

ATR-FTIR Analysis of CT Secondary Structure Changes under LFMF Exposure. We then examined the enzyme secondary structure by ATR-FTIR spectroscopy. The typical ATR-FTIR spectra of the free CT and MNP-CT conjugates before, immediately after, and 3 h after LFMF exposure are presented in Figure 7. The positions of the amide I and II absorption bands in the spectra provided overall information on the peptide bond oscillations. The protein secondary structure was assessed by comparing the second derivatives of the spectra for the amide I band with the literature data for the native CT molecule.[36,37] The fractions of alpha-, beta-, and random structures were estimated by deconvoluting the amide I band curves. The details of the deconvolution analysis and FTIR spectra are presented in Supporting Information (Figures S12−S14). We could not assess the possible aggregation of MNP-CT conjugates during the experiment, and therefore, deconvolution analysis did not account for protein aggregation, which is a limitation.

The secondary structure of the native CT was in good agreement with the literature (11% alpha-helices, 55% beta-sheets, and beta-turns, and 34% random structures[38]) (Table 3). There were little or no changes in the secondary structure elements of the enzyme after its conjugation to either type of functionalized MNPs. The secondary structure of the native CT did not change after the magnetic field exposure, which was consistent with no change in its catalytic activity. In contrast, in both MNP-CT conjugates, the enzyme secondary structure was noticeably altered by the LFMF. In both cases, we observed nearly complete disappearance of α-helices immediately after the exposure, which restored to the initial values after 3 h. The fraction of β-structures in MNP-Cy-CT decreased from 54 to 40% but practically did not change in MNP-LA-CT. The β-structures in MNP-Cy-CT did not restore after the field exposure. The random element fractions increased in MNP-LA-CT and MNP-Cy-CT from 41 to 47% and 34 to 57%, respectively, which was completely reversible and restored to initial values 3 h after the field exposure. Thus, the exposure of the MNP-CT conjugates to the LFMF produced substantial changes in the CT secondary structure, which was either completely reversible (MNP-LA-CT) or partially reversible (MNP-Cy-CT). The observed structural changes appeared to be consistent with the catalytic activity changes.

Table 3. Changes in the Immobilized CT Secondary Structure Occurring under LFMF Exposure (Based on Figures S11−S13)

secondary structure element	treatments	native CT	MNP-LA-CT	MNP-Cy-CT
α-helices, %	before LFMF	10	9	12
	immediately after LFMF	13	1	3
	3 h after LFMF		11	12
β-sheets and β-strands, %	before LFMF	53	48	54
	immediately after LFMF	59	51	40
	3 h after LFMF		49	43
random structure, %	before LFMF	37	41	34
	immediately after LFMF	28	47	57
	3 h after LFMF		40	46

DISCUSSION

Prior analysis of changes in the rates of biocatalytic reactions upon application of LFMF has centered on physical models considering the mechanical motion of MNPs.[13,18,24] These models suggest that the alternating current magnetic field induces rotational−vibrational motion due to Brownian relaxation of MNPs.[18,39] The moving MNPs can exert mechanical forces upon the conjugated enzyme molecules. As a result, the enzyme secondary structure[18] (or its interaction with MNP-conjugated inhibitors[18]) can change, leading to changes in the rate of the catalyzed reaction. In this consideration, the MNPs act like force-creating machines

https://doi.org/10.1021/acsomega.2c00704
ACS Omega 2022, 7, 20644−20655

actuated by the magnetic field, and the changes in the reaction rates are explained by the force-induced alterations in the enzyme secondary structure. Due to the involvement of the nanoparticle mechanical motion, this type of response to the magnetic field is called magneto−nanomechanical actuation.[19] In this study, we posit that Brownian relaxation of MNPs leads to stimulation of the conjugated enzyme molecules by magneto−nanomechanical forces. As a result of such stimulation, the secondary structure of enzyme molecules was disturbed, and the enzyme activity decreased.

The present work supplements the theoretical analyses by two types of experiments. The first one is in silico using MD simulations to assess enzyme evolution upon application of stretching forces. The second one is in vitro using UV−vis and ATR-FTIR spectroscopies to measure the reaction rates and protein secondary structure. Two types of MNP-CT conjugates were synthesized, in which the enzyme was conjugated to either LA- or Cy-functionalized gold-coated MNPs. Different surface functionalization allowed us to engage different functional groups in the protein molecule. In both cases, we used conditions producing conjugates with each CT molecule attached to multiple MNPs to maximize the effects of their mechanical motion.[18] The MD simulations of radially directed stretching forces applied to either carboxylic or amino groups of CT suggested the possibility for deformation (shrinking) of the substrate-binding site, but essentially no change in the catalytic triad. The experimental measurements of the actual rates of enzymatic hydrolysis of a specific substrate by both types of MNP-CT conjugates demonstrated that the Michaelis−Menten constant increased while the catalytic constant remained unchanged after application of LFMF. This observation appears to be consistent with the result of the MD simulations.

The analysis of the secondary structure of the enzyme by ATR-FTIR spectroscopy suggested nearly complete loss of α-helices and increase in random structures in MNP-CT conjugates after the application of the LFMF. This further reinforces the validity of magneto−nanomechanical analysis. Notably, there were differences in the responses of different conjugates: the carboxylic group-conjugated CT displayed stronger changes in the secondary structure than the amino group-conjugated enzyme. This result seems to be consistent with the difference in the changes in the reaction rates and Michaelis−Menten constants for these two conjugates. Needless to say, that both the enzyme activity and conformation measurements were conducted not contemporaneous but after application of the magnetic field. This represents a limitation of our study since magnetic field-induced deformations can be reversed. However, these measurements were conducted within 3 min after the magnetic field application, which allowed us to examine the slower relaxation processes. Indeed, the changes in the reaction rates and the enzyme secondary structure are reversible and restore 3 h after the end of the magnetic field exposure. The restoration seems to be complete for the amino group-conjugated CT that is less affected by the field and partial for the carboxylic group-conjugated enzyme that is more affected by the field. The timescale of protein relaxation may depend on multiple factors such as the number of amino acids, the molecular mass, and the secondary structure.[40,41] The α-helices fold more rapidly than the β-structures or random elements.[41] Interestingly, the 3 h refolding time was observed for chymotrypsinogen, an inactive precursor of CT denatured in the reductive media that cleaved the disulfide bonds.[42] Consistent with these prior observations, we observed the full restoration of α-helices in both MNP-CT conjugates and either partial or full restoration of β-structures and random elements within 3 h after LFMF treatment of MNP-LA-CT and MNP-Cy-CT. Therefore, the magnetic field can produce reversible and/or partially irreversible inactivation and changes in the conformation, depending on the points of attachment and, possibly, sites of force application in MNP-CT conjugates.

It has been shown previously that application of the stretching forces to enzyme globules using magnetic tweezers decreases the catalytic activity due to deterioration of substrate binding in enzyme-active sites.[7,43] These changes in the enzyme structure and catalytic activity were reversible. Such behavior, similar to the phenomenon we observed, could be explained by greater flexibility of the enzyme globule regions responsible for the substrate binding.[44,45] This flexibility is needed to ensure broader substrate specificity of the enzyme with respect to structurally different compounds.[46] At the same time, the precise positioning of the residues in the catalytic site is needed to enable the catalytic turnover.

We would like to point to several limitations of this study. Due to a limited calculation capacity the time scale of the MD experiment (20 ns) is much less than that of the magnetic force application ∼1 ms (estimated as the duration of the oscillation front of the magnetic field[25]). However, the MD simulation experiment revealed that the changes important for catalysis might occur during first 0.2−0.3 ns, and then, the enzyme structure remains the same. Thus, we suppose that 20 ns trajectories during MD simulation experiment can predict real CT behavior while magneto−nanomechanical forces are applied to a single molecule. In a catalytic system containing multiple enzymes during the magnetic field exposure time, these multiple molecules undergo thousands of cycles of such stresses. The measurable catalytic activity and conformation properties are mean of such multiple contributions, which is underscored by their slow relaxation times observed in this study.

Also, in the kinetic experiment, the observed changes in the Michaelis−Menten constants in our MNP-CT conjugates are relatively small, from 1.6 to 2.5-fold, which is less than the changes observed because of enzyme conjugation to MNPs during preparation of these conjugates. There was a considerable change in the enzyme kinetics after CT conjugation with over 10-fold loss of enzyme activity ($V_{max}/[E]_o$) along with 5.6- or 30-fold decrease in the Michaelis−Menten constant. Since charge interactions between the substrate and functionalized MNPs can play a significant role in enzymatic reaction rates,[32−34] changes in the CT localization at the nanoparticle surface produced by the mechanical motion of the MNPs in the magnetic field could in theory account for some changes in the reaction rate. We also would like to point out that our MNP-CT conjugate samples are heterogeneous, and some of the enzyme molecules may be "unproductively" linked to the MNPs with only portion of enzyme molecules being sensitive to the motion of the nanoparticles. Since the measured kinetic parameters are mean for the entire conjugated enzyme population, the actual magnitude of the magneto−nanomechanical effects could be far greater than we have measured. Future studies would need to optimize the conjugation strategies to produce uniform and highly responsive biocatalytic systems. We believe that such

https://doi.org/10.1021/acsomega.2c00704
ACS Omega 2022, 7, 20644−20655

remotely actuated systems can find applications in advanced manufacturing, nanomedicine, and other areas.

CONCLUSIONS

Herein, modulation of CT conjugated to MNPs by LFMF was studied (1) in silico by MD of enzyme behavior under stretching forces and (2) in vitro by spectroscopic analysis of CT activity and secondary structure. MD simulation of CT behavior under applying stretching forces to accessible amino or carboxylic groups revealed that the overall conformation was conservative. However, we observed changes in the distance between atoms of polypeptide chains forming the entrance to the substrate-binding pocket. At the same time, the applied forces did not change the arrangement of the catalytic triad. From the enzyme's activity point of view, such changes in the enzyme secondary structure could affect substrate binding but not the substrate catalytic conversion.

We synthesized two types of MNP-CT conjugates where either amine or carboxylic groups of the enzyme were modified. As a result of the conjugation reaction, CT molecules were bound to at least two nanoparticles, as suggested by NTA and TEM analyses. Under applied LFMF, the catalytic activity of both types of conjugated CT was decreased. This was a result of increasing K_M while k_{cat} remained constant. Moreover, we observed changes in the secondary structure of conjugated CT. The effect of LFMF was restorable/partially restorable, depending on the type of MNP-CT conjugates. We posit that such changes were a result of the magneto−nanomechanical action of MNPs in LFMF.yugolovin@yandex.ru

ASSOCIATED CONTENT

Supporting Information

The Supporting Information is available free of charge at https://pubs.acs.org/doi/10.1021/acsomega.2c00704.

Additional theoretical/experimental details and methods (PDF)

Visualization of CT behavior under exposure of stretching forces (ZIP)

AUTHOR INFORMATION

Corresponding Authors

Alexander V. Kabanov − *School of Chemistry, Lomonosov Moscow State University, Moscow 119991, Russia; Center for Nanotechnology in Drug Delivery, Eshelman School of Pharmacy, University of North Carolina at Chapel Hill, Chapel Hill, North Carolina 27599-7362, United States;* orcid.org/0000-0002-3665-946X; Email: kabanov@email.unc.edu

Natalia L. Klyachko − *School of Chemistry, Lomonosov Moscow State University, Moscow 119991, Russia; Center for Nanotechnology in Drug Delivery, Eshelman School of Pharmacy, University of North Carolina at Chapel Hill, Chapel Hill, North Carolina 27599-7362, United States;* orcid.org/0000-0002-9357-8236; Email: klyachko@enzyme.chem.msu.ru

Authors

Maxim M. Veselov − *School of Chemistry, Lomonosov Moscow State University, Moscow 119991, Russia;* orcid.org/0000-0002-8983-2772

Igor V. Uporov − *School of Chemistry, Lomonosov Moscow State University, Moscow 119991, Russia*

Maria V. Efremova − *School of Chemistry, Lomonosov Moscow State University, Moscow 119991, Russia; National University of Science and Technology "MISIS", Moscow 119049, Russia; Department of Applied Physics, Eindhoven University of Technology, Eindhoven 5600 MB, The Netherlands;* orcid.org/0000-0002-5196-5596

Irina M. Le-Deygen − *School of Chemistry, Lomonosov Moscow State University, Moscow 119991, Russia;* orcid.org/0000-0002-6366-4491

Andrey N. Prusov − *A.N. Belozersky Research Institute, Moscow 119991, Russia*

Igor V. Shchetinin − *National University of Science and Technology "MISIS", Moscow 119049, Russia*

Alexander G. Savchenko − *National University of Science and Technology "MISIS", Moscow 119049, Russia*

Yuri I. Golovin − *School of Chemistry, Lomonosov Moscow State University, Moscow 119991, Russia; G.R. Derzhavin Tambov State University, Tambov 392000, Russia*

Complete contact information is available at: https://pubs.acs.org/10.1021/acsomega.2c00704

Author Contributions

A.V.K., Y.I.G., and N.L.K. made a contribution to experiment conceptualization. I.V.U. performed MD simulation experiments. M.V.E. synthesized MNPs. M.M.V. synthesized MNP-CT conjugates and analyzed enzymatic kinetics. I.M.L. analyzed ATR-FTIR spectra. A.N.P. took TEM measurements of MNPs. I.V.S., M.V.E., and A.G.S. took and analyzed Mössbauer spectra. M.M.V. and A.V.K. wrote the manuscript.

Notes

The authors declare no competing financial interest.

ACKNOWLEDGMENTS

This work was supported by the Russian Science Foundation grants 22-13-00261 and 20-63-46029. This work was supported in part by the Lomonosov Moscow State University (Registration Theme AAAA-A21-121011290089-4). The authors also acknowledge Lomonosov Moscow State University Development Program PNR 5.13.

REFERENCES

(1) Agarwal, P. K. Enzymes: An integrated view of structure, dynamics and function. *Microb. Cell Factories* **2006**, *5*, 2.

(2) Chang, C.-e.; Huang, Y.-m.; Mueller, L.; You, W. Investigation of Structural Dynamics of Enzymes and Protonation States of Substrates Using Computational Tools. *Catalysts* **2016**, *6*, 82.

(3) Warshel, A.; Bora, R. P. Perspective: Defining and quantifying the role of dynamics in enzyme catalysis. *J. Chem. Phys.* **2016**, *144*, 180901.

(4) Henzler-Wildman, K. A.; Thai, V.; Lei, M.; Ott, M.; Wolf-Watz, M.; Fenn, T.; Pozharski, E.; Wilson, M. A.; Petsko, G. A.; Karplus, M.; Hübner, C. G.; Kern, D. Intrinsic motions along an enzymatic reaction trajectory. *Nature* **2007**, *450*, 838−844.

(5) Klibanov, A. M.; Samokhin, G. P.; Martinek, K.; Berezin, I. V. Enzymatic mechanochemistry: a new approach to studying the mechanism of enzyme action. *Biochim. Biophys. Acta* **1976**, *438*, 1−12.

(6) Puchner, E. M.; Alexandrovich, A.; Kho, A. L.; Hensen, U.; Schäfer, L. V.; Brandmeier, B.; Gräter, F.; Grubmüller, H.; Gaub, H. E.; Gautel, M. Mechanoenzymatics of titin kinase. *Proc. Natl. Acad. Sci.* **2008**, *105*, 13385−13390.

(7) Guo, Q.; He, Y.; Lu, H. P. Interrogating the activities of conformational deformed enzyme by single-molecule fluorescence-magnetic tweezers microscopy. *Proc. Natl. Acad. Sci.* **2015**, *112*, 13904−13909.

(8) Pal, N.; Wu, M.; Lu, H. P. Probing conformational dynamics of an enzymatic active site by an in situ single fluorogenic probe under piconewton force manipulation. *Proc. Natl. Acad. Sci.* **2016**, *113*, 15006−15011.
(9) Hughes, M. L.; Dougan, L. The physics of pulling polyproteins: a review of single molecule force spectroscopy using the AFM to study protein unfolding. *Rep. Prog. Phys.* **2016**, *79*, 076601.
(10) Noy, A. *Handbook of Molecular Force Spectroscopy*; Springer: New York, 2008.
(11) Zaltron, A.; Merano, M.; Mistura, G.; Sada, C.; Seno, F. Optical tweezers in single-molecule experiments. *Eur. Phys. J. Plus* **2020**, *135*, 896.
(12) Vilfan, I. D.; Kamping, W.; van den Hout, M.; Candelli, A.; Hage, S.; Dekker, N. H. An RNA toolbox for single-molecule force spectroscopy studies. *Nucleic Acids Res.* **2007**, *35*, 6625−6639.
(13) Klyachko, N. L.; Sokolsky-Papkov, M.; Pothayee, N.; Efremova, M. V.; Gulin, D. A.; Pothayee, N.; Kuznetsov, A. A.; Majouga, A. G.; Riffle, J. S.; Golovin, Y. I.; Kabanov, A. V. Changing the enzyme reaction rate in magnetic nanosuspensions by a non-heating magnetic field. *Angew. Chem., Int. Ed. Engl.* **2012**, *51*, 12016−12019.
(14) Andreeva, Y. I.; Drozdov, A. S.; Avnir, D.; Vinogradov, V. V. Enzymatic Nanocomposites with Radio Frequency Field-Modulated Activity. *ACS Biomater. Sci. Eng.* **2018**, *4*, 3962−3967.
(15) An, J.; Li, G.; Zhang, Y.; Zhang, T.; Liu, X.; Gao, F.; Peng, M.; He, Y.; Fan, H. Recent Advances in Enzyme-Nanostructure Biocatalysts with Enhanced Activity. *Catalysts* **2020**, *10*, 338.
(16) Xiong, R.; Zhang, W.; Zhang, Y.; Zhang, Y.; Chen, Y.; He, Y.; Fan, H. Remote and real time control of an FVIO-enzyme hybrid nanocatalyst using magnetic stimulation. *Nanoscale* **2019**, *11*, 18081−18089.
(17) Collins, C. B.; Riskowski, R. A.; Ackerson, C. J. Radiofrequency remote control of thermolysin activity. *Sci. Rep.* **2021**, *11*, 6070.
(18) Efremova, M. V.; Veselov, M. M.; Barulin, A. V.; Gribanovsky, S. L.; Le-Deygen, I. M.; Uporov, I. V.; Kudryashova, E. V.; Sokolsky-Papkov, M.; Majouga, A. G.; Golovin, Y. I.; Kabanov, A. V.; Klyachko, N. L. In Situ Observation of Chymotrypsin Catalytic Activity Change Actuated by Nonheating Low-Frequency Magnetic Field. *ACS Nano* **2018**, *12*, 3190−3199.
(19) Golovin, Y. I.; Gribanovsky, S. L.; Golovin, D. Y.; Klyachko, N. L.; Majouga, A. G.; Master, A. M.; Sokolsky, M.; Kabanov, A. V. Towards nanomedicines of the future: Remote magneto-mechanical actuation of nanomedicines by alternating magnetic fields. *J. Controlled Release* **2015**, *219*, 43−60.
(20) Bender, M. L.; Kezdy, F. J.; Wedler, F. C. Alpha-chymotrypsin: enzyme concentration and kinetics. *J. Chem. Educ.* **1967**, *44*, 84−88.
(21) Achstetter, T.; Ehmann, C.; Wolf, D. H. New proteolytic enzymes in yeast. *Arch. Biochem. Biophys.* **1981**, *207*, 445−454.
(22) MacKerell, A. D., Jr.; Banavali, N.; Foloppe, N. Development and current status of the CHARMM force field for nucleic acids. *Biopolymers* **2000**, *56*, 257−265.
(23) Nemukhin, A. V.; Gariev, I. A.; Rogov, A. V.; Varfolomeev, S. D. Serine hydrolase catalytic sites : geometry invariants and modeling catalytic activity. *Mendeleev Commun.* **2006**, *16*, 290−292.
(24) Majouga, A.; Sokolsky-Papkov, M.; Kuznetsov, A.; Lebedev, D.; Efremova, M.; Beloglazkina, E.; Rudakovskaya, P.; Veselov, M.; Zyk, N.; Golovin, Y.; Klyachko, N.; Kabanov, A. Enzyme-functionalized gold-coated magnetite nanoparticles as novel hybrid nanomaterials: synthesis, purification and control of enzyme function by low-frequency magnetic field. *Colloids Surf., B* **2015**, *125*, 104−109.
(25) Golovin, Y. I.; Klyachko, N. L.; Majouga, A. G.; Gribanovskii, S. L.; Golovin, D. Y.; Zhigachev, A. O.; Shuklinov, A. V.; Efremova, M. V.; Veselov, M. M.; Vlasova, K. Y.; Usvaliev, A. D.; Le-Deygen, I. M.; Kabanov, A. V. New Approaches to Nanotheranostics: Polyfunctional Magnetic Nanoparticles Activated by Non-Heating Low-Frequency Magnetic Field Control Biochemical System with Molecular Locality and Selectivity. *Nanotechnol. Russ.* **2018**, *13*, 215−239.
(26) Landers, J.; Salamon, S.; Remmer, H.; Ludwig, F.; Wende, H. Simultaneous Study of Brownian and Néel Relaxation Phenomena in Ferrofluids by Mössbauer Spectroscopy. *Nano Lett.* **2016**, *16*, 1150−1155.
(27) Golovin, Y. I.; Klyachko, N. L.; Majouga, A. G.; Sokolsky, M.; Kabanov, A. V. Theranostic multimodal potential of magnetic nanoparticles actuated by non-heating low frequency magnetic field in the new-generation nanomedicine. *J. Nanoparticle Res.* **2017**, *19*, 63.
(28) Mørup, S.; Topsøe, H. Mössbauer studies of thermal excitations in magnetically ordered microcrystals. *Appl. Phys.* **1976**, *11*, 63−66.
(29) Demchenko, P.; Nedelko, N.; Mitina, N.; Lewińska, S.; Dłużewski, P.; Greneche, J. M.; Ubizskii, S.; Navrotskyi, S.; Zaichenko, A.; Ślawska-Waniewska, A. Collective magnetic behavior of biocompatible systems of maghemite particles coated with functional polymer shells. *J. Magn. Magn Mater.* **2015**, *379*, 28−38.
(30) Mahato, K.; Nagpal, S.; Shah, M. A.; Srivastava, A.; Maurya, P. K.; Roy, S.; Jaiswal, A.; Singh, R.; Chandra, P. Gold nanoparticle surface engineering strategies and their applications in biomedicine and diagnostics. *3 Biotech* **2019**, *9*, 57.
(31) Tsu, C. A.; Perona, J. J.; Schellenberger, V.; Turck, C. W.; Craik, C. S. The substrate specificity of Uca pugilator collagenolytic serine protease 1 correlates with the bovine type I collagen cleavage sites. *J. Biol. Chem.* **1994**, *269*, 19565−19572.
(32) Wu, C.-S.; Wu, C.-T.; Yang, Y.-S.; Ko, F.-H. An enzymatic kinetics investigation into the significantly enhanced activity of functionalized gold nanoparticles. *Chem. Commun.* **2008**, 5327−5329.
(33) You, C.-C.; Agasti, S. S.; De, M.; Knapp, M. J.; Rotello, V. M. Modulation of the Catalytic Behavior of α-Chymotrypsin at Monolayer-Protected Nanoparticle Surfaces. *J. Am. Chem. Soc.* **2006**, *128*, 14612−14618.
(34) Pandey, P.; Singh, S. P.; Arya, S. K.; Gupta, V.; Datta, M.; Singh, S.; Malhotra, B. D. Application of Thiolated Gold Nanoparticles for the Enhancement of Glucose Oxidase Activity. *Langmuir* **2007**, *23*, 3333−3337.
(35) O'Neil, M. J. *The Merck Index*, 15th ed.; Royal Society of Chemistry: Cambridge, U.K., 2013.
(36) Venyaminov, S. Y.; Kalnin, N. N. Quantitative IR spectrophotometry of peptide compounds in water (H2O) solutions. I. Spectral parameters of amino acid residue absorption bands. *Biopolymers* **1990**, *30*, 1243−1257.
(37) Yang, H.; Yang, S.; Kong, J.; Dong, A.; Yu, S. Obtaining information about protein secondary structures in aqueous solution using Fourier transform IR spectroscopy. *Nat. Protoc.* **2015**, *10*, 382−396.
(38) Vinogradov, A. A.; Kudryashova, E. V.; Grinberg, V. Y.; Grinberg, N. V.; Burova, T. V.; Levashov, A. V. The chemical modification of alpha-chymotrypsin with both hydrophobic and hydrophilic compounds stabilizes the enzyme against denaturation in water-organic media. *Protein Eng.* **2001**, *14*, 683−689.
(39) Golovin, Y. I.; Gribanovskii, S. L.; Golovin, D. Y.; Klyachko, N. L.; Kabanov, A. V. Single-domain magnetic nanoparticles in an alternating magnetic field as mediators of local deformation of the surrounding macromolecules. *Phys. Solid State* **2014**, *56*, 1342.
(40) Naganathan, A. N.; Muñoz, V. Scaling of folding times with protein size. *J. Am. Chem. Soc.* **2005**, *127*, 480.
(41) Ivankov, D. N.; Finkelstein, A. V. Prediction of protein folding rates from the amino acid sequence-predicted secondary structure. *Proc. Natl. Acad. Sci.* **2004**, *101*, 8942.
(42) Duda, C. T.; Light, A. Refolding of bovine threonine-neochymotrypsinogen. *J. Biol. Chem.* **1982**, *257*, 9866.
(43) Guo, Q.; He, Y.; Lu, H. P. Manipulating and probing enzymatic conformational fluctuations and enzyme-substrate interactions by single-molecule FRET-magnetic tweezers microscopy. *Phys. Chem. Chem. Phys.* **2014**, *16*, 13052.
(44) Weng, Y.-Z.; Chang, D. T.; Huang, Y. F.; Lin, C. W. A study on the flexibility of enzyme active sites. *BMC Bioinf.* **2011**, *12*, S32.
(45) James, M. N.; Sielecki, A.; Salituro, F.; Rich, D. H.; Hofmann, T. Conformational flexibility in the active sites of aspartyl proteinases revealed by a pepstatin fragment binding to penicillopepsin. *Proc. Natl. Acad. Sci.* **1982**, *79*, 6137.

https://doi.org/10.1021/acsomega.2c00704
ACS Omega 2022, 7, 20644−20655

(46) Saranya, N.; Selvaraj, S. Variation of protein binding cavity volume and ligand volume in protein-ligand complexes. *Bioorg. Med. Chem. Lett.* **2009**, *19*, 5769.

https://doi.org/10.1021/acsomega.2c00704
ACS Omega 2022, 7, 20644−20655